Paper # 070LT-0383 **Topic: Laminar Flames**

8th US National Combustion Meeting
Organized by the Western States Section of the Combustion Institute
and hosted by the University of Utah
May 19-22, 2013.

Laminar Burning Speed of *n*-Hexane-Air Mixtures

S. Coronel[1] *R. Mével*[1] *P. Vervish*[1] *P. A. Boettcher*[1] *V. Thomas*[1]
N. Chaumeix[2] *N. Darabiha*[3] *J. E. Shepherd*[1]

[1]*Graduate Aeronautical Laboratories,*
California Institute of Technology, Pasadena, Ca 91125

[2]*Institut de Combustion, Aérothermique, Réactivité et Environnement,*
CNRS, Orléans, France

[3]*Laboratoire EM2C-CNRS UPR 288,*
École Centrale Paris, Châtenay-Malabry, France

n-Hexane is an easy-to-use fuel for laboratory investigations of hydrocarbon vapor explosions and has been used widely as a surrogate for commodity fuels such as kerosene. As part of our ongoing studies into flammability hazards in aircraft environments, we have been carrying out experiments at reduced pressure, below 100 kPa, in order to measure ignition and flame propagation in *n*-hexane-air mixtures. The objectives of the present study were to study experimentally the effects of composition, initial temperature, and initial pressure on the burning speed of *n*-hexane-air mixtures. Our study expands on and complements existing data and compares the experimental measurements with numerical predictions from various chemical models. The laminar burning speed of *n*-hexane-air mixtures was measured experimentally using the spherically expanding flame technique. The effects of equivalence ratio, initial temperature and initial pressure were investigated in the ranges: Φ = 0.75–1.7, T_1 = 295–380 K and P_1 = 40–100 kPa, respectively. A typical inverted U-shaped curve was obtained for the evolution of the burning speed as a function of equivalence ratio. At a fixed composition, the burning speed increases as the initial temperature increases and as the initial pressure decreases; this is in agreement with previous burning speed studies done using n-alkanes, from C_5 to C_8. Three detailed reaction models, the JetSurF model, the model of Ramirez et al., and the Caltech model were evaluated with respect to the present data. The present study indicated that among the models tested, the JetSurF model is the most accurate model for evaluating *n*-hexane-air mixtures.

1 Introduction

Ignition of fuel-air mixtures in the fuel tank or surrounding flammable leakage zones is a main safety concern for the commercial aviation industry [1]. During the flight phases of an aircraft, the pressure within the fuel tank varies between 0.2 atm to 1 atm. In order to assess the risk of an accidental combustion event during the flight phases of an aircraft, it is necessary to characterize properties such as the burning speed of fuel-air mixtures over a wide range of initial pressures. *n*-Hexane has been extensively used in our laboratory as a single component surrogate of kerosene [1–3]. Although more representative surrogates can be used for kerosene [4–6], *n*-hexane exhibits a relatively high vapor pressure which facilitates experimenting at ambient temperature. In contrast to *n*-heptane, which has been widely studied, *n*-hexane oxidation has received little

interest [7]. Curran et al. [8] studied hexane isomer chemistry by measuring and modeling exhaust gases from an engine. The ignition delay-time behind a shock wave was measured by Burcat et al. [9] and Zhukov et al. [10]. Boettcher et al. [1] studied the effect of the heating rate on the low temperature oxidation of hexane by air, and the minimum temperature of a heated surface required to ignite hexane-air mixtures [3]. Bane [2] measured the minimum ignition energy of several hexane-air mixtures. A limited number of studies have been found on the laminar burning speed of *n*-hexane-air mixtures. Davis and Law [11] measured the laminar burning speed of *n*-hexane-air mixtures at ambient conditions using the counterflow twin flame technique. Farrell et al. [12] used pressure traces from spherically expanding flames to determine the burning speed of *n*-hexane-air mixtures at an initial temperature and initial pressure of 450 K and 304 kPa, respectively. Kelley et al. [13] reported experimental measurements using spherically expanding flames at an initial temperature of 353 K and initial pressures of 100 kPa to 1000 kPa. Ji et al. [14] used the counterflow burner technique to measure the burning speed of *n*-hexane-air mixtures at an initial temperature and initial pressure of 353 K and 100 kPa. In contrast to previous work, the present study focuses on initial conditions below atmospheric pressure in order to simulate aircraft fuel tank conditions.

2 Experimental Setup

The experiments were performed in a 22 liter stainless steel cylindrical vessel 30 cm in height and diameter. Two parallel flanges were used to mount the electrodes for the ignition system. The flames were ignited using a capacitive discharge through a transformer to create a spark between two electrodes. The circuit is described in detail by Kwon et al. [15]. The ignition system generated a spark with energy on the order of 300 mJ across 2–4 mm spark gaps. The electrodes were made out of tungsten wire and were 0.38 mm in diameter. Two other parallel flanges held BK7 glass windows that were 11.7 cm in diameter to allow for schlieren and shadowgraphic visualization of the flame propagation. A high-speed camera was used to record the flame propagation at a rate of 10,000 frames per second with a resolution of 512×512. Figure 1 shows an example of a spherically expanding flame obtained in the present study. Before each experiment, the vessel was evacuated to less than 10 Pa. High purity liquid *n*-hexane was injected through a septum and vaporized, nitrogen and oxygen were then added using the method of partial pressures. A static pressure manometer was used to measure the gas pressure inside the vessel to within 0.01 kPa, allowing for precise determination of the mixture composition. The mixture was thoroughly mixed using a magnetically-driven fan mixer and was allowed to come to rest by waiting a fixed amount of time before igniting the mixture. The pressure evolution during the combustion event in the vessel was measured using a thermally-protected piezoresistive pressure transducer.

3 Burning Speed Measurement

Asymptotic theoretical analyses [16–18] performed in the limit of high activation energy, and assuming a linear relation between the stretched and unstretched burning speeds in the low stretch rate regime, lead to

$$S_L = S_L^0 - L \cdot K, \tag{1}$$

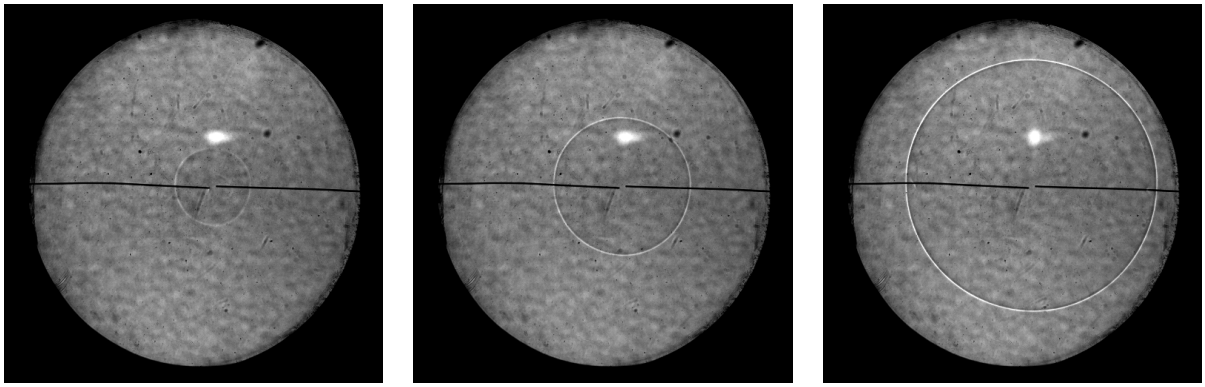

t = 5.0 ms t = 9.7 ms t = 17.1 ms

Figure 1: Spherical expanding flame propagation in a *n*-hexane-air mixture at Φ = 0.9 and initial temperature and initial pressure of 393 K and 50 kPa, respectively.

where S_L and S_L^0 are the stretched and the unstretched laminar burning speeds, respectively, L is the Markstein length and K is the stretch rate. In the case of a large volume vessel and for measurements limited to the initial period of propagation where the flame radius is small, the pressure increase can be neglected [19], therefore the burning speed and the spatial velocity are linked only through the expansion ratio accross the flame front

$$S_L = \frac{V_S}{\sigma}. \tag{2}$$

The expansion ratio, σ, is defined as

$$\sigma = \frac{\rho_u}{\rho_b}, \tag{3}$$

where ρ_u and ρ_b are the densities of the unburned and burned gases, respectively. Substituting Equation 1 into Equation 2 yields

$$V_S = \frac{dR_f}{dt} = V_S^0 - \sigma L \cdot K. \tag{4}$$

where V_S^0 is the unstretched spatial flame velocity and R_f is the flame radius. The stretch rate is obtained from the following equation [20, 21]:

$$K = \frac{1}{A} \cdot \frac{dA}{dt} = \frac{1}{R_f^2} \cdot \frac{dR_f^2}{dt} = \frac{2}{R_f} \cdot \frac{dR_f}{dt} = 2 \cdot \frac{V_S}{R_f}, \tag{5}$$

where A is the flame surface area. Combining Equation 4 and Equation 5 and integrating for $R_f \ll D_{exp}$, where D_{exp} is the characteristic dimension of the experimental set-up, the unstretched flame speed with respect to time and flame radius is:

$$V_S^0 \cdot t = R_f + 2 \cdot L \cdot ln\,(R_f) + C. \tag{6}$$

where C is an integration constant.

Equation 7 is found by normalizing Equation 6 with the final flame radius, $R_{f,final}$,

$$V_S^0 \cdot (t_f - t) = R_f - R_{f,final} + 2 \cdot L \cdot ln\left(\frac{R_f}{R_{f,final}}\right) + C. \quad (7)$$

The unstretched laminar burning speed is then obtained by dividing the unstretched flame speed by the expansion ratio as shown in Equation 2.

A Matlab routine, described in [22], was used to obtain the flame radius as a function of time to derive V_S^0. A mask is first applied over an image to remove the background (electrodes), edge detection is then used to identify the expanding flame edge. A binary value of 0 indicates the background and a binary value of 1 indicates the flame edge. An ellipse is fitted to the detected flame edge; the ellipse parameters are then used to obtain an equivalent radius. Finally, a linear least-square regression is applied to the radius data to obtain the unstretched flame speed, and the Markstein length. The method used to estimate the uncertainty of the laminar burning speed and the Markstein length is described in [22].

4 Experimental Results

To validate the present results, a set of experiments were performed at an initial temperature and initial pressure of 296 K and 100 kPa, respectively, and compared with previous studies. The present study results are shown in Figure 2 (a) along with results previously obtained by Davis and Law [11]. A two-tailed z-test was performed using the present data and the Davis and Law [11] data to test two hypotheses, $H_0 : \mu_1 = \mu_2$ and $H_a : \mu_1 \neq \mu_2$, where μ_1 is the mean of the present data and μ_2 is the mean of the Davis and Law [11] data. The z-test results indicated that the null hypothesis, H_0, cannot be rejected. The difference between the means of the two data sets is zero at the α = 0.02 confidence level, therefore supporting the validity of the present results. The results from Kelley et al. [13] and from Ji et al. [14], obtained at a higher initial temperature of 353 K, are shown in Figure 2 (b). For equivalence ratios in the range Φ = 0.80–1.25, the burning speeds measured at an initial temperature of 353 K are higher (50% higher at Φ = 0.80 and 18% higher at Φ = 1.25) than those measured at an initial temperature of 296 K. This is expected due to the increase of the flame temperature, and thus of the overall reaction rate. The difference between the burning speeds, at an initial temperature of 296 K and those obtained by Ji et al. [14] at an initial temperature of 353 K, decreases as the equivalence ratio increases past Φ = 1.25. The burning speeds obtained by Kelley et al. [13] at an initial temperature of 353 K remain higher on the rich side when compared to the respective burning speeds at an initial temperature of 296 K, 16 % higher at Φ = 1.40 and 25% higher at Φ = 1.50.

The evolution of the burning speed as a function of equivalence ratio was studied at an initial pressure of 50 kPa. Figure 3 shows the present study results obtained at initial pressures of 100 kPa and 50 kPa and previous results obtained by Davis and Law [11]. The uncertainty associated with the burning speed measurements, on the order of 5%, makes it difficult to differentiate between the results obtained at an initial pressure of 50 kPa and those obtained at an initial pressure of 100 kPa. Using a t-test, at the α = 0.2 confidence level, there is a statistically significant difference between

the burning speeds at an initial pressure of 50 kPa and the burning speeds at an initial pressure of 100 kPa. Qualitatively, a slight increase of the burning speed with the decrease of the initial pressure can be observed, this trend is characteristic of alkane-air mixtures [13].

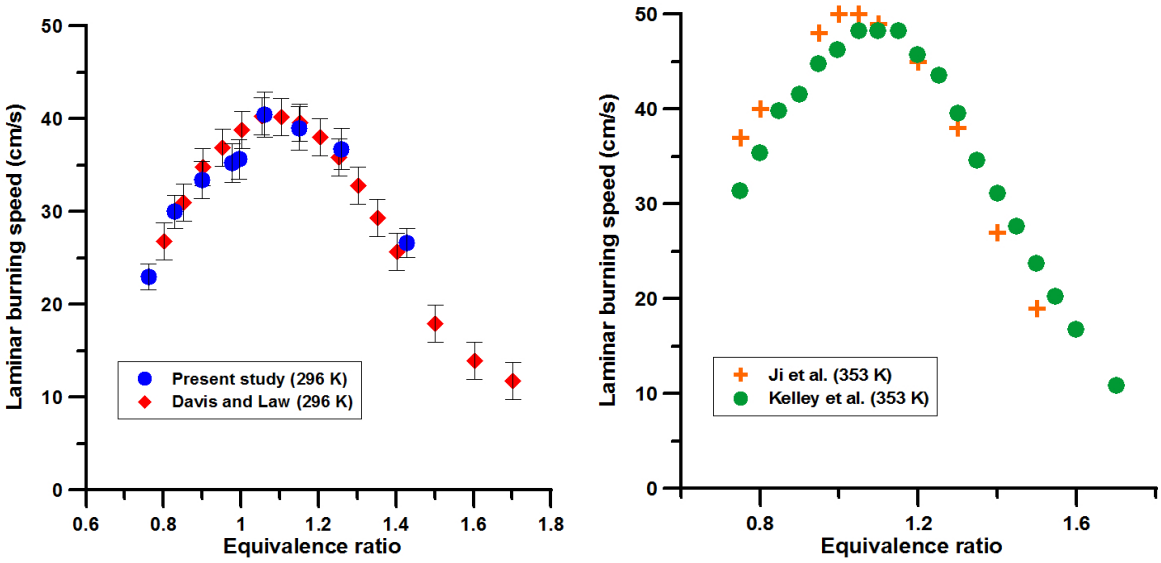

(a) T_1 = 296 K (b) T_1 = 353 K

Figure 2: Experimental laminar burning speed of *n*-hexane-air mixtures as a function of equivalence ratio at an initial pressure of 100 kPa.

The effect of initial temperature was studied at an initial pressure of 50 kPa and three equivalence ratios, Φ = 0.90, Φ = 1.10 and Φ = 1.40. The results are shown in Figure 4 (a). At initial temperatures of 296 K to 380 K, the burning speed was observed to increase 47% at Φ = 1.00 and 64% at Φ = 0.90. The lean mixtures exhibit the highest rate of burning speed increase (0.27 cm/s.K) with initial temperature increase, whereas the rich mixtures exhibit the lowest rate of burning speed increase (0.18 cm/s.K) with initial temperature increase. The effect of initial pressure on the burning speed has been investigted at Φ = 0.90 at an initial temperature of 353 K. The results are shown in Figure 4 (b) along with the results of Kelley et al. [13] obtained at initial pressures of 100 kPa to 1000 kPa. The laminar burning speed is seen to decrease significantly with the increase of the initial pressure, 20% between 50 and 100 kPa and 53% between 50 and 1000 kPa,. This evolution can be represented by a power law: $S_L^0(P) = 129 \times P^{-0.24}$. This dependency of the burning speed with the initial pressure is in agreement with thermal flame theory of Mallard and Le Chatelier [23], assuming a global reaction order of 1.5. At an initial pressure of 50 kPa, the theoretical laminar burning speed is within 4% of the experimental results, and at an initial pressure of 1000 kPa, the theoretical laminar burning speed is within 9% of the experimental results.

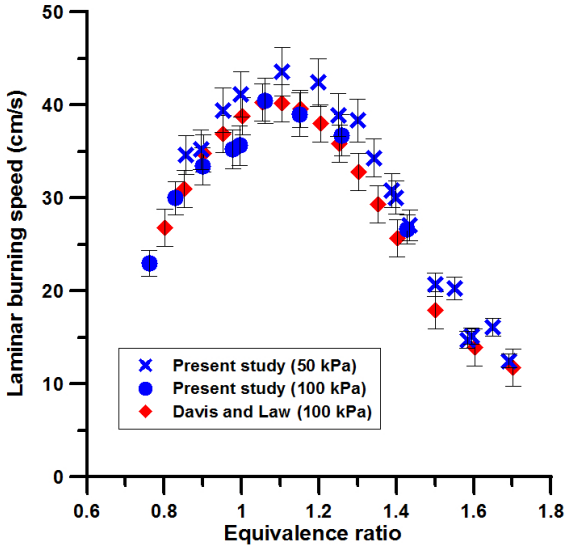

Figure 3: Experimental laminar burning speed of *n*-hexane-air mixtures as a function of equivalence ratio at an initial temperature of 296 K and initial pressures of 50 kPa and 100 kPa.

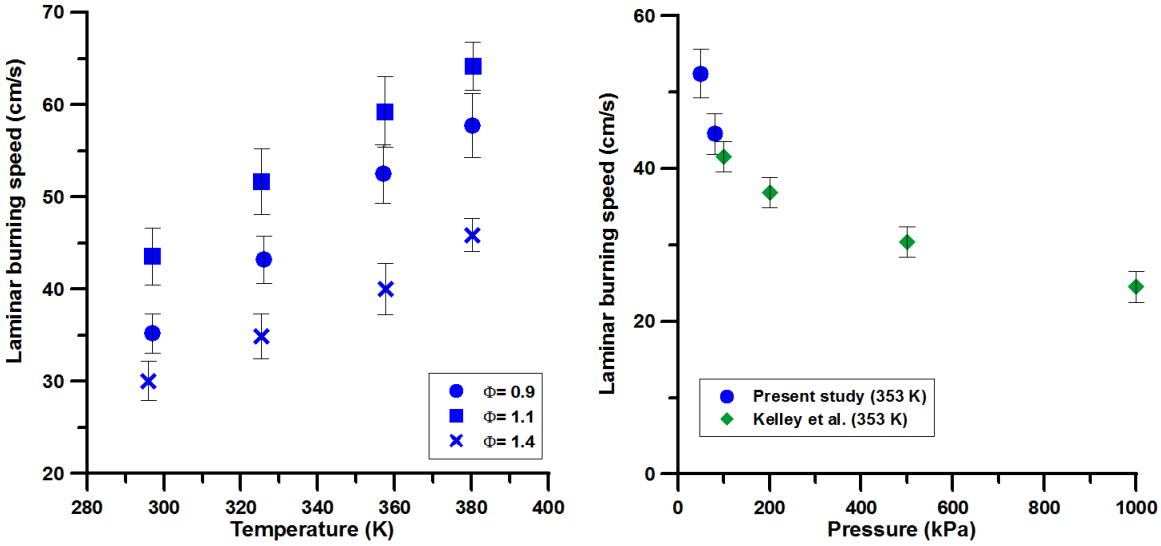

(a) Effect of temperature (P_1 = 50 kPa) (b) Effect of pressure (Φ = 0.90)

Figure 4: Experimental laminar burning speed of *n*-hexane-air mixtures as a function of initial temperature and pressure.

Figure 5 shows the variation of the Marsktein length with equivalence ratio at an initial temperature and initial pressure of 296 K and 50 kPa, respectively. Lean and rich mixtures exhibit large positive (0.3 mm) and negative (-0.5 mm) Markstein lengths, respectively. The transition from positive to negative Markstein length values occurs at $\Phi \approx 1.30$. This trend is consistent with previous Markstein length data obtained for C_5 to C_8 *n*-alkane-air mixtures [13]. Figure 6 shows examples of a stable lean mixture and an unstable rich mixture flame propagation. In the lean mixture shown in Figure 6 (a), the flame front remains smooth and undisturbed during the propagation within the field of view ($R_f \leq R_w$), where R_w is the window radius. In the rich mixture shown in Figure 6 (b), the flame front becomes progressively more disturbed as it grows and exhibits significant cellular structure before the flame exits the field of view. The development of the cellular pattern is apparently due to thermo-diffusive instabilities that are characteristic of rich hydrocarbon-air mixtures [24].

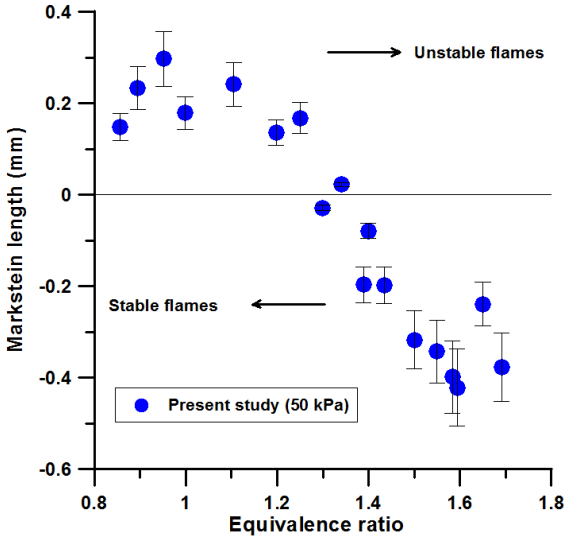

Figure 5: Evolution of the Marsktein length for *n*-hexane-air mixtures as a function of equivalence ratio at an initial temperature and initial pressure of 296 K and 50 kPa, respectively.

The temporal evolution of the pressure and the peak explosion pressure in the vessel were examined for *n*-hexane-air mixtures at an initial temperature and initial pressure of 296 K and 50 kPa, respectively. The explosion pressure versus time exhibits a rise to a peak pressure on the order of 100 ms for *n*-hexane-air mixtures, followed by an exponential decay. An example of a typical pressure trace is given in Figure 7 for a *n*-hexane-air mixture at $\Phi = 1.44$. In the example shown, a maximum pressure rise rate of 450 MPa/s is observed.

The effect of the equivalence ratio on the peak explosion pressure was studied at $\Phi = 0.62$–1.60. The measured peak explosion pressure is shown in Figure 8 (a) as a function of equivalence ratio along with the theoretical curve given by constant volume, adiabatic, equilibrium calculations performed using Cantera [25]. The measured values are lower than the theoretical values since heat losses are not taken into account in the calculations. The constant volume calculation overpredicts

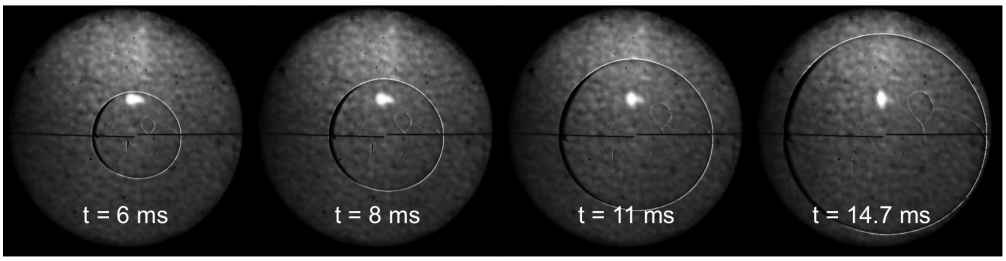

(a) $\Phi = 0.91$

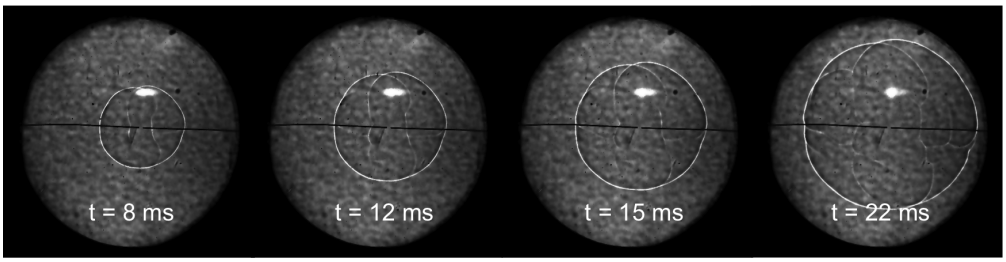

(b) $\Phi = 1.65$

Figure 6: Example of stable and unstable flame propagations of *n*-hexane-air mixtures at an initial temperature and initial pressure of 296 K and 50 kPa, respectively.

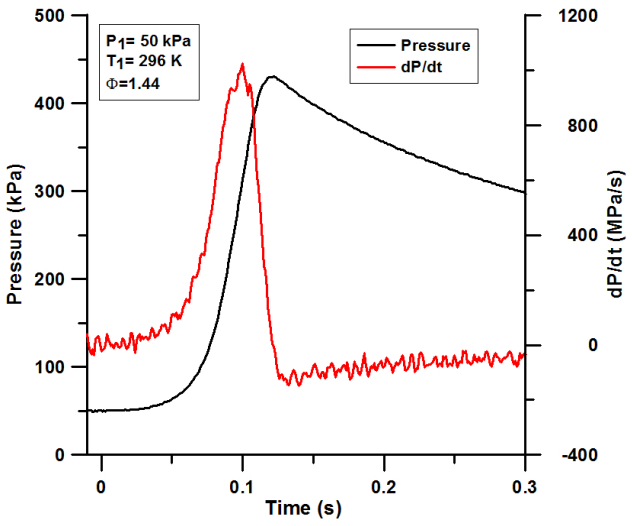

Figure 7: Example of a pressure signal and pressure derivative for a rich *n*-hexane-air mixture.

the peak pressure by, 12% for a stoichiometric (Φ = 1.00) mixture and 13% for a rich (Φ = 1.60) mixture. The peak pressure follows a trend similar to that of the laminar burning speed as a function of equivalence ratio. The peak pressure increases with equivalence ratio from Φ = 0.70 and reaches a maximum value of 474 kPa on the rich side at Φ = 1.23, after which the peak pressure decreases. This behavior was previously observed by Boettcher [3] in hexane-air mixtures at an initial temperature and initial pressure of 296 K and 100 kPa, respectively. In the present study and Boettcher's study, the peak pressure reaches a maximum value at $\Phi \approx$ 1.2–1.3.

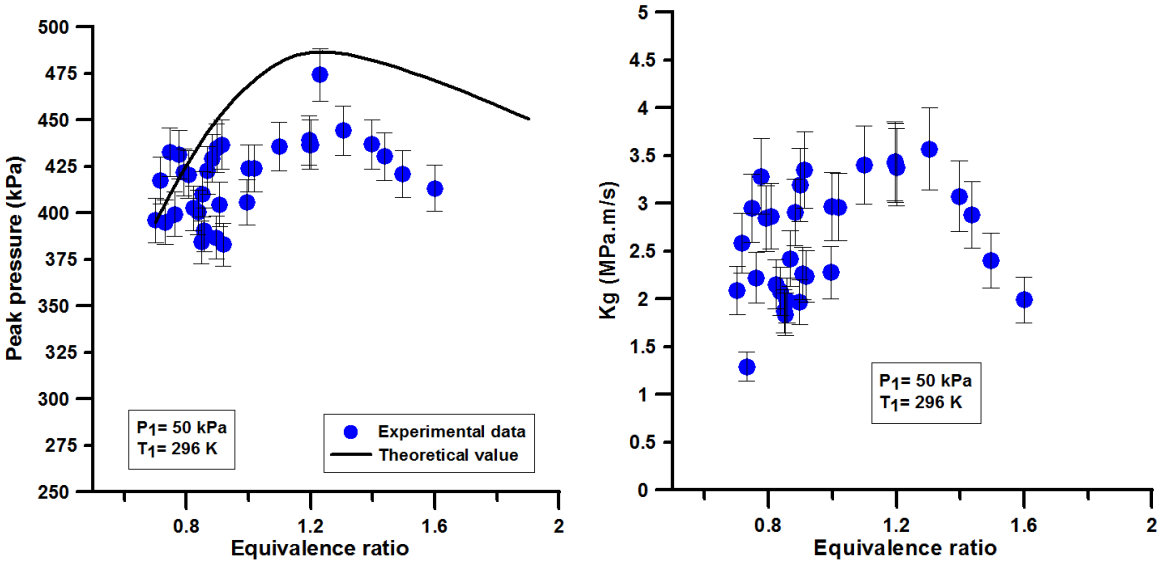

Figure 8: (a) Peak pressure and (b) pressure rise coefficient, K_g, for *n*-hexane-air mixtures as a function of equivalence ratio.

The pressure rise coefficient, K_g, shown in Equation 8 is calculated as the cubic root of the combustion vessel volume multiplied by the maximum time derivative of the pressure.

$$K_g = V^{\frac{1}{3}} \cdot \left(\frac{dp}{dt}\right)_{max} \tag{8}$$

The parameter describes closed vessel combustion and is used to characterize the explosivity of a mixture. This value allows for comparison of maximum pressure rise rates for different gases for a fixed vessel geometry and volume and is commonly used for hazard assessment [26]. To estimate the derivate shown in Equation 8, the numerically differentiated combustion pressure trace was filtered using a Savitzkye-Golay filter with a fifth-order polynomial and 11 data points. The results of K_g are shown in Figure 8 (b) as a function of the equivalence ratio along with the uncertainty ranges for *n*-hexane-air mixtures at an initial temperature and initial pressure of 296 K and 50 kPa, respectively. The value of K_g ranged from 1.3 MPa.m/s at Φ = 0.73 to 3.6 MPa.m/s at Φ = 1.30. K_g increases with increasing equivalence ratio in the range Φ = 0.62–1.00. For higher equivalence ratios, K_g remains nearly constant at 3.5 MPa.m/s. The magnitude of K_g peaks near Φ = 1.30.

In addition, with changes in the initial temperature from 296 K to 380 K at an initial pressure of 50 kPa, the coefficient K_g varies between, 2.2–3.2 MPa.m/s at Φ = 0.90, 3.1–3.4 MPa.m/s at Φ = 1.10, and 2.6–3.1 MPa.m/s at Φ = 1.40. Finally, the coefficient K_g increases with increasing pressure, from 50 kPa to 100 kPa. Using an 11.25 liter combustion vessel at an initial temperature and initial pressure of 100 kPa and 295 K, respectively, Kunz [26] obtained K_g values of 1.4–3.9 MPa.m/s (Φ = 0.70–1.00) for methane-air mixtures, 2.3–6.6 MPa.m/s (Φ = 0.74–1.00) for ethane-air mixtures, 2.0–4.0 MPa.m/s (Φ = 0.75–0.95) for propane-air mixtures and 9.1 MPa.m/s (Φ = 0.93) for a hydrogen-air mixture. In the present study, K_g values of 1.3–3.0 MPa.m/s were found for equivalence ratios in the range Φ = 0.73–1.00. The K_g values for hexane-air mixtures at an initial temperature and initial pressure of 296 K and 50 kPa, respectively, are comparable to the K_g values of methane-air mixtures and lower than the K_g values of ethane-air (76–120% lower) mixtures, propane-air (33–55% lower) mixtures and hydrogen-air mixtures (180% lower) at an initial temperature and initial pressure of 296 K and 100 kPa, respectively.

5 Modeling Results

Three detailed reaction models, the JetSurF model [27], with 2163 reactions and 348 species, the Ramirez et al. model [28], with 1789 reactions and 401 species, and the Caltech model [29], with 1119 reactions and 155 species, were evaluated with respect to the present data and previous study data. The Caltech model [29] which has been validated extensively for a wide range of hydrocarbons including *n*-heptane and *n*-dodecane, was extended to include the chemistry of *n*-hexane. The sub-mechanism for *n*-hexane was obtained by reducing the detailed *n*-alkane model from the Lawrence Livermore National Laboratory, LLNL, [30] using the Directed Relation Graph with Error Propagation method, DRGEP, [31]. The modeling of the laminar burning speed was achieved using the Regath software [32]. Regath is a Fortran 90 package which includes thermodynamics and chemical routines. It also includes a 0-D reactor solver as well as a 1-D freely-propagating flame solver and a counterflow solver.

Figures 9–11 compare the predictions of the three detailed models to the experimental results from the present study and from the literature [11, 13, 14]. The JetSurF model [27], shown by the small dashed lines, reproduces the experimental results for the lean and stoichiometric mixtures but underestimates the burning speed obtained for the rich mixtures by 30–40 %. The model of Ramirez et al. [28], shown by large dashed lines, systematically underestimates the experimental results by up to a factor of two for the rich mixtures at an initial pressure of 50 kPa. The Caltech model [29], shown by the solid line, overestimates the burning speed by 15–20% for lean and stoichiometric mixtures. For the rich mixtures, an overlap is found between the predictions of the Caltech model [29] and the experimental results. Table 1 shows the average differences between the experimental burning speeds and the calculated burning speeds using the JetSurF model [27], the model of Ramirez et al. [28] and the Caltech model [29], P_1 is the initial pressure and T_1 is the initial temperature. The difference between the predicted JetSurF model [27] burning speeds and the experimental burning speeds are on average low (8%) over a range of conditions. Whereas, the difference between the predicted burning speeds using model of Ramirez et al. [28] and the experimental burning speeds are on average high (23%) over a range of conditions. All three models capture the trends observed experimentally: (i) an inverted U-shaped curve for the evolution of the

burning speed with the equivalence ratio, (ii) increase in the burning speed as the initial temperature increases and (iii) as the initial pressure decreases. Overall, the present study indicated that the JetSurF model [27] is the most accurate model for the prediction of burning speeds of *n*-hexane-air mixtures.

Condition	JetSurF	Ramirez et al.	Caltech
P_1 = 100 kPa and T_1 = 296 K, varying Φ	8%	25%	11%
P_1 = 100 kPa and T_1 = 353 K, varying Φ	7%	21%	13%
P_1 = 50 kPa and T_1 = 296 K, varying Φ	14%	27%	12%
P_1 = 50 kPa and Φ = 0.90, Φ = 1.10, Φ = 1.40, varying T_1	7%	20%	9%
T_1 = 296 K and Φ = 0.90, varying P_1	6%	24%	14%

Table 1: Average differences between the experimental laminar burning speeds and the calculated laminar burning speeds

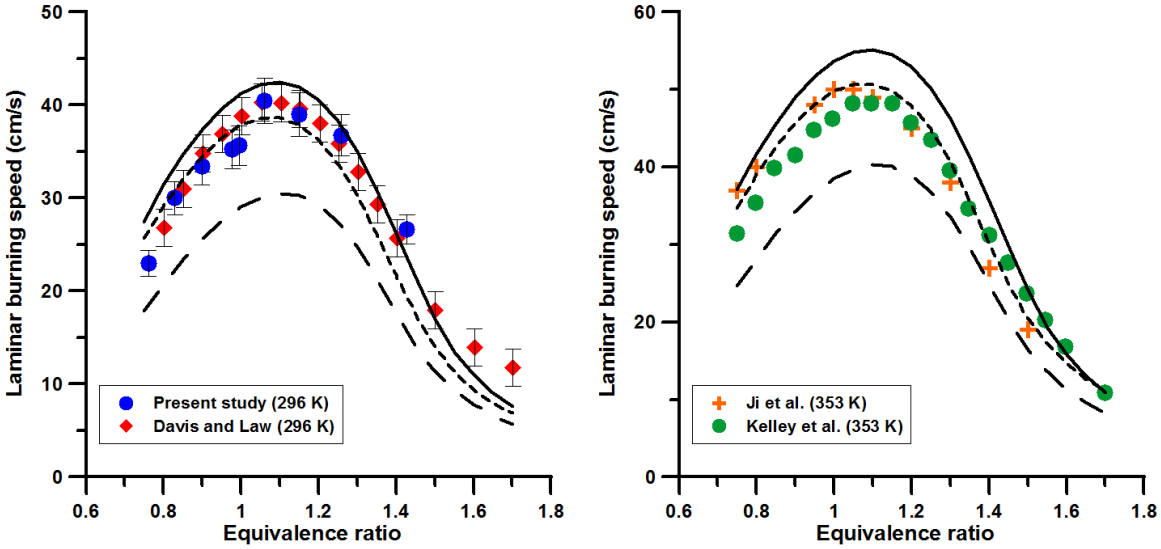

(a) T_1=296 K (b) T_1=353 K

Figure 9: Experimental and calculated laminar burning speed of *n*-hexane-air mixtures as a function of equivalence ratio at an initial pressure of 100 kPa. JetSurf [27]: - - - - - - - - ; Ramirez et al. [28]: — — — ; Caltech [29]: ———— .

A reaction pathway analysis was performed using Cantera [25] for a lean *n*-hexane-air mixture at $\Phi = 0.90$ and initial temperature and initial pressure of 296 K and 50 kPa, respectively, using the JetSurF reaction model [27]. The burning speeds calculated with Regath [32] and Cantera [25] were within 0.3 cm/s, which represents a difference of less than 1%. The reaction pathway was obtained as elementary mass fluxes and was performed with a threshold of 10% in order to focus on the most important pathways. Figure 12 shows a typical example of a reaction pathway obtained at a distance of 4.9 mm from the flame front and a corresponding temperature of 1443

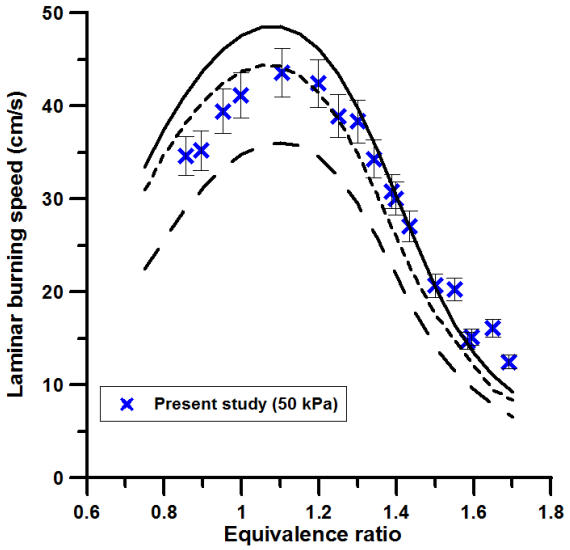

Figure 10: Experimental and calculated laminar burning speed of *n*-hexane-air mixtures as a function of equivalence ratio at an initial temperature and initial pressure of 296 K and 50 kPa, respectively. JetSurf [27]: - - - - - - - - ; Ramirez et al. [28]: — — — ; Caltech [29]: ———— .

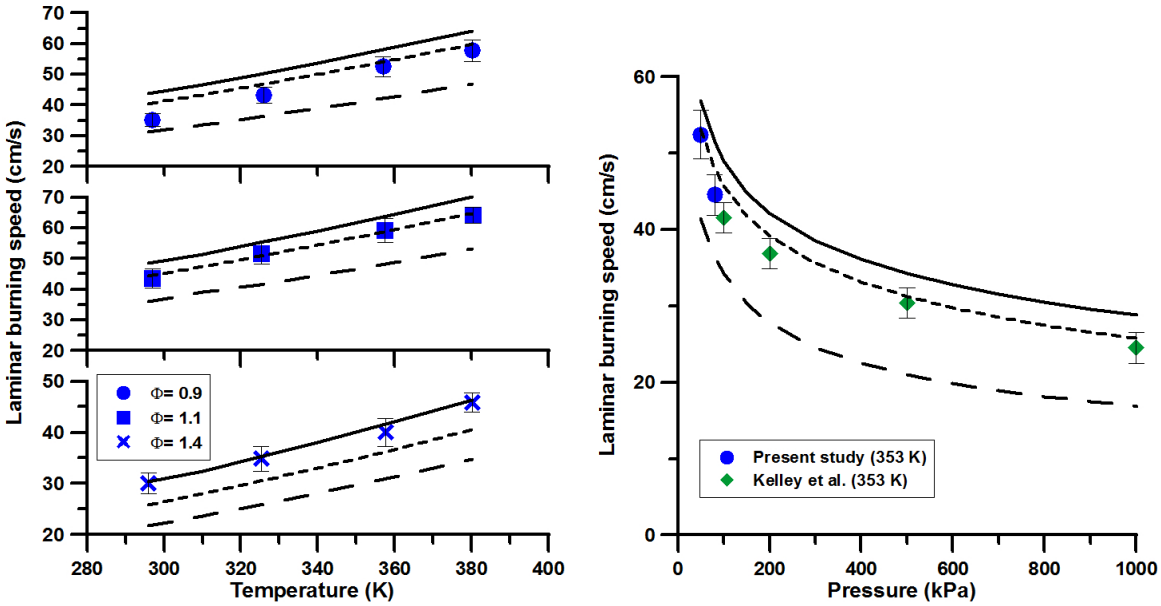

(a) Effect of temperature (P_1 = 50 kPa) (b) Effect of pressure (Φ = 0.9)

Figure 11: Experimental and calculated laminar burning speed of *n*-hexane-air mixtures as a function of initial temperature and initial pressure. JetSurf [27]: - - - - - - - - ; Ramirez et al. [28]: — — — ; Caltech [29]: ———— .

K. Hexane consumption is mainly driven by H-abstraction reactions, with the OH radical being the most efficient abstracter. During this first step, abstraction occurs from either carbon at the same rate. The 1-hexyl radical undergoes isomerization which increases the yields of 2-hexyl and 3-hexyl radicals. Conversely, hexane undergoes C-C bond fission leading to ethyl, propyl and butyl radicals. The consumption of 2-hexyl and 3-hexyl radicals also occurs mainly through C-C bond rupture which leads to a significant amount of C_2H_4. Ethylene consumption eventually leads to CO formation mainly though the following sequences:

$$C_2H_4 \xrightarrow{OH} C_2H_3 \xrightarrow{OH} C_2H_2 \xrightarrow{O} HCCO \xrightarrow{O_2} CO \tag{9}$$

and

$$C_2H_4 \xrightarrow{OH} C_2H_3 \xrightarrow{O_2} CH_2CO \xrightarrow{H} CH_3 \xrightarrow{O} CH_2O \xrightarrow{OH} HCO \xrightarrow{OH} CO. \tag{10}$$

At the temperature considered, no significant conversion of CO into CO_2 was detected. This reaction pathway analysis underlines the importance of ethylene which appears as a "bottle-neck" species in the course of hexane oxidation.

6 Conclusion

In the present study, *n*-hexane-air mixtures have been characterized through experimental measurements and calculations of the laminar burning speed and explosion pressure. The effect of equivalence ratio, temperature and pressure on the burning speed were investigated experimentally by varying the equivalence ratio Φ = 0.62–1.60, the initial temperature from 296 K to 380 K and the initial pressure from 50 kPa to 100 kPa. The pressure rise coefficient, an indicator of the explosivity of a mixture, was shown to fluctuate with changes in the initial temperature (296–380 K) at an initial pressure of 50 kPa, the coefficient K_g ranges between 2.2–3.2 MPa.m/s at Φ = 0.90, 3.1–3.4 MPa.m/s at Φ = 1.10, and 2.6–3.1 MPa.m/s at Φ = 1.40. Additional tests would be required to properly assess the trend of K_G as a function of the mixture's initial temperature. An increase in the initial pressure from 50 kPa to 100 kPa increases the pressure rise coefficient from 2.9 MPa.m/s to 19.3 MPa.m/s (570% increase) at Φ = 1.44. It was demonstrated that calculations using the JetSurF model [27] could predict the laminar burning speed on average to within 8% of the experimental value. The Caltech model [29] could predict the laminar burning speed on average to within 12% of the experimental value. On the other hand, the model of Ramirez et al. [28] significantly underestimated the burning speed at the conditions tested; on average, the predictions came to within 23% of the experimental values. Overall, the JetSurF model [27] demonstrated to be the most reliable model to use for *n*-hexane-air mixtures since it had a better agreement with the experimental results over a range of compositions, initial temperatures and initial pressures, than the Caltech model [29] and the model of Ramirez et al [28].

Acknowledgments

The present work was carried out in the Explosion Dynamics Laboratory of the California Institute of Technology and was supported by The Boeing Company through a Strategic Research and Development Relationship Agreement CT-BA-GTA-1.

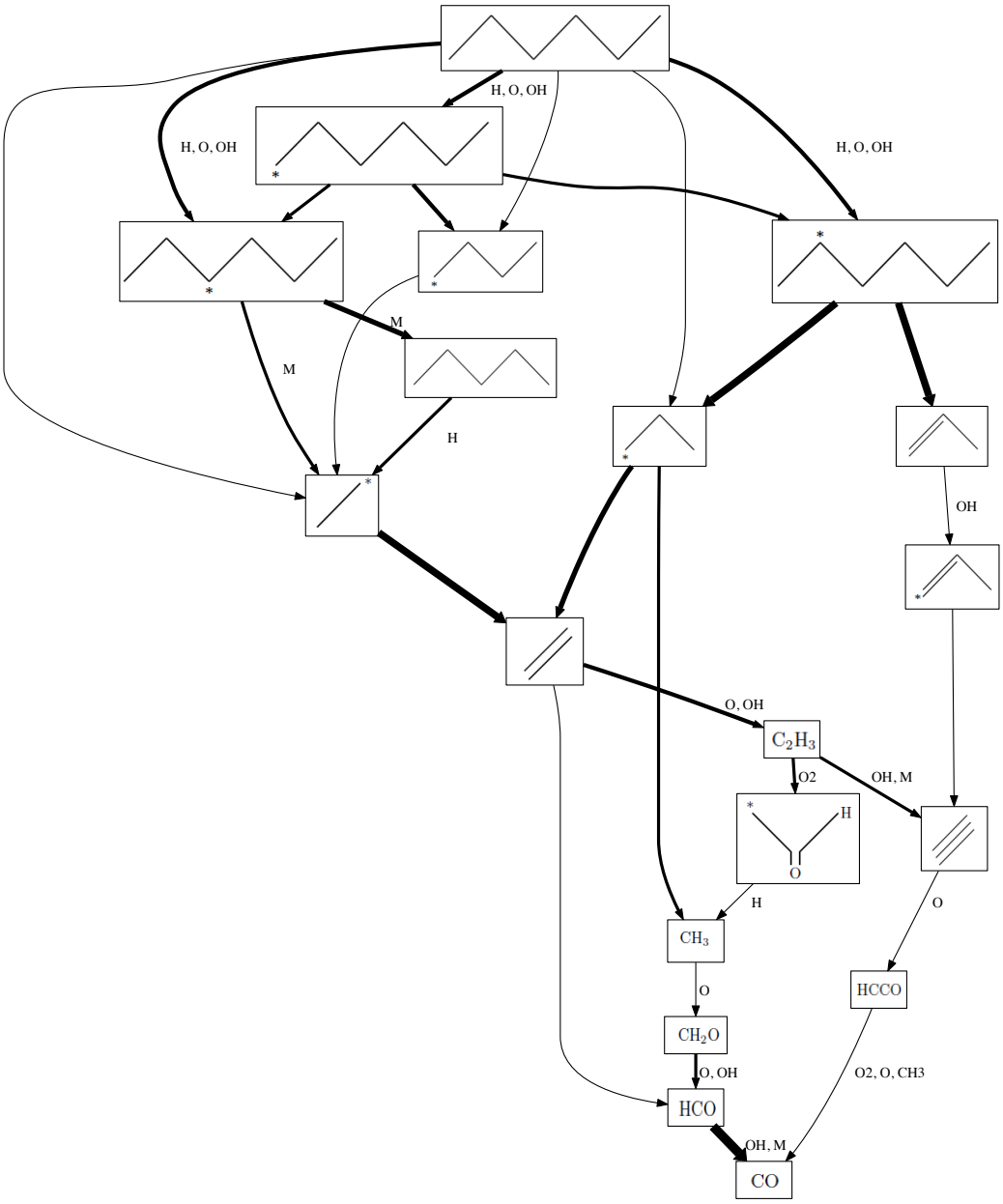

Figure 12: Reaction pathway analysis for the carbon element in a lean *n*-hexane-air flame at Φ = 0.90 and initial temperature and initial pressure of 296 K and 50 kPa, respectively. Position and temperature in the flame are 4.9 mm and 1443 K, respectively.

References

[1] P. A. Boettcher, R. Mével, V. Thomas, and J. E. Shepherd. *Fuel*, 96 (2012) 392–403.

[2] S.P.M. Bane. *Spark ignition: experimental and numerical investigation with application to aviation safety*. PhD thesis, Califronia Institute of Technology, 2010.

[3] P.A. Boettcher. *Thermal Ignition*. PhD thesis, California Institute of Technology, 2012.

[4] P. Dagaut and M. Cathonnet. *Progress in Energy and Combustion Science*, 32 (2006) 48–92.

[5] P. Dagaut, A. El Bakali, and A. Ristori. *Fuel*, 85 (2006) 944–956.

[6] S. Dooley, S.H. Wona, M. Chaos, J. Heyne, Y. Ju, F.L. Dryer, K. Kumar, C.-J. Sung, H. Wang, M.A. Oehlschlaeger, R.J. Santoro, and T.A. Litzinger. *Combustion and Flame*, 157 (2010) 2333–2339.

[7] J. Simmie. *Progress in Energy and Combustion Science*, 29 (2003) 599–634.

[8] H.J. Curran, P. Gaffuri, W.J. Pitz, C.K. Westbrook, and W.R. Leppard. Autoignition chemistry of the hexane isomers: an experimental and kinetic modelling study. In *SAE International Fuels and Lubricants Meeting and Exposition*, 1995.

[9] A. Burcat, E. Olchanski, and C. Sokolinski. *Israel Journal of Chemistry*, 36 (1996) 313–320.

[10] V. P. Zhukov, V. A. Sechenov, and A. Yu. Starikovskii. *Combustion and Flame*, 136 (2004) 257–259.

[11] S.G. Davis and C.K. Law. *Combustion Science and Technology*, 140 (1998) 427–449.

[12] J. Farrell, R. Johnston, and I. Androulakis. Molecular structure effects on laminar burning velocities at elevated temperature and pressure. In SAE Technical Paper, 2004. 2004-01-2936.

[13] A. P. Kelley, A. J. Smallbone, D. L. Zhu, and C. K. Law. *Proceedings of the Combustion Institute*, 33 (2011) 963–970.

[14] C. Ji, E. Dames, Y.l. Wang, H. Wang, and F.N. Egolfopoulos. *Combustion and Flame*, 157 (2010) 277–287.

[15] E. Kwon, S. P. Moffett, J. E. Shepherd, and A. C. Day. Combustion characteristics of hydrogen as used in a flammable test mixture. In *Proceedings of the International Conference on Lightning and Static Electricity 2007*, 2007. Paper PPR-48.

[16] G.I. Sivashinsky. *Acta Astronautica 3 (1976)*, 3 (1976) 889–918.

[17] M. Matalon and B.J. Matkowsky. *Journal of Fluid Mechanics*, 124 (1982) 239–259.

[18] P. Clavin. *Progress in Energy and Combustion Science*, 11 (1985) 1–59.

[19] X. J. Gu D. Bradley, P. H. Gaskell. *Combustion and Flames*, 104 (1996) 176–198.

[20] N. Lamoureux, N. Djebali-Chaumeix, and C.E. Paillard. *Experimental Thermal and Fluid Science*, 27 (2003) 385–393.

[21] K.T. Aung, M.I. Hassan, and G.M. Faeth. *Combustion and Flame*, 109 (1997) 1–24.

[22] R. Mével, F. Lafosse, N. Chaumeix, G. Dupré, and C. E. Paillard. *International Journal of Hydrogen Energy*, 34 (2009) 9007–9018.

[23] K. K. Kuo. *Principles of Combustion*. John Wiley & Sons, USA, 1986.

[24] G. Jomaas, C.K. Law, and J.K. Bechtold. *Journal of Fluid Mechanics*, 583 (2007) 1–26.

[25] D. Goodwin. Cantera: An object-oriented software toolkit for chemical kinetics, thermodynamics, and transport processes. http://code.google.com/p/cantera/.

[26] O. Kunz. Combustion characteristics of hydrogen- and hydrocarbon-air mixtures in closed vessels. Master's thesis, California Institute of Technology, 1998.

[27] H. Wang, E. Dames, B. Sirjean, D.A. Sheen, R. Tangko, A. Violi, J.Y.W. Lai, F.N. Egolfopoulos, D.F. Davidson, R.K. Hanson, C.T. Bowman, C.K. Law, W. Tsang, N.P. Cernansky, D. L. Miller, and R.P. Lindstedt. A high-temperature chemical kinetic model of n-alkane (up to n-dodecane), cyclohexane, and methyl-, ethyl-, n-propyl and n-butyl-cyclohexane oxidation at high temperatures, jetsurf version 2.0, september 19, 2010 (http://melchior.usc.edu/jetsurf/jetsurf2.0).

[28] H.P. Ramirez, K. Hadj-Ali, P. Dievart, G. Dayma, C. Togbe, G. Moreac, and P. Dagaut. *Proceedings of the Combustion Institute*, 33 (2011) 375–382.

[29] G. Blanquart, P. Pepiot-Desjardins, and H. Pitsch. *Combustion and Flame*, 156 (2009) 588–607.

[30] C. K. Westbrook, W. J. Pitz, O. Herbinet, H. J. Curran, and E. J. Silke. *Combustion and Flame*, 156 (2009) 181–199.

[31] P. Pepiot and H. Pitsch. *Combustion and Flame*, 154 (2008) 67–81.

[32] S. Candel, T. Schmitt, and N. Darabiha. In *23rd International Colloquium on the Dynamics of Explosions and Reactive Systems*, Irvine, CA., July 2011.